Journal of Energy Storage 1 (2015) 44–53

Contents lists available at ScienceDirect

Journal of Energy Storage

journal homepage: www.elsevier.com/locate/est

Nonlinear aging characteristics of lithium-ion cells under different operational conditions

Simon F. Schuster [a,*], Tobias Bach [b], Elena Fleder [b], Jana Müller [b], Martin Brand [a], Gerhard Sextl [b], Andreas Jossen [a]

[a] Institute for Electrical Energy Storage Technology, Technische Universität München, Arcisstraße 21, 80333 Munich, Germany
[b] Fraunhofer Institute for Silicate Research, Neunerplatz 2, 97082 Würzburg, Germany

ARTICLE INFO

Article history:
Received 16 March 2015
Received in revised form 27 April 2015
Accepted 6 May 2015
Available online 22 May 2015

Keywords:
cyclic aging
nonlinear
2nd-life
reuse
lithium plating

ABSTRACT

The potential reuse of lithium-ion batteries exhausted upon electric vehicle operation is a broadly discussed topic. However, a profound understanding of battery aging behavior is a prerequisite to assess overall system cost and economic benefit of battery reuse: Whereas the capacity fade under load is commonly reported to show a linear dependency on charge throughput, a turning point to nonlinear aging characteristics is observed at residual capacities of about 80% under different operational conditions. Based on a widespread aging matrix, results indicate an earlier appearance of nonlinear characteristics at high charging rates and operational voltage windows but low temperatures. Scanning electron microscopy images reveal areas of thick surface films at the anode while the cathode stays unmodified. Therefore, a thickening of the solid electrolyte interphase, catalyzed by oxidation products migrating to the anode, is believed to be the dominating aging mechanism before the turning point. Afterwards, lithium plating might even occur at moderate temperatures and charging rates due to deteriorated ionic kinetics and graphite active material loss. As all these mechanisms are dependent on the cell potential, an optimized operational strategy may avoid or retard nonlinear aging characteristics and extend the life of lithium-ion cells.

1. Introduction

Although a global wide introduction of battery electric vehicles (BEV) is regarded as an inevitable next step to lower the emission of greenhouse gases, the product acceptance of potential customers are still rather low. Due to the high price of BEV resulting from the costly battery storages, barely 2% of newly registered cars in Germany in 2013 were pure or hybrid electric [1]. Despite a growing need due to a possible lithium scarcity in the future, a reduction of the price achieved by recycling of disused batteries in not economically feasible for now [2]. Therefore, a potential reuse of lithium-ion batteries exhausted upon BEV operation is a broadly discussed topic, e.g. in the context of 2nd-life-applications like stationary energy storage [3–9]. Using aged batteries to reduce grid-strengthening investments, for frequency sustainment issues or as an interim storage for renewable energies, promises high revenue potentials [5,6]. However, a profound understanding and predictability of battery aging behavior is a prerequisite to assess overall system cost and economic benefit of battery reuse.

In general, the consequences of aging in lithium-ion cells are the loss of capacity, the increase of impedance and the reduction of the maximum power due to a higher polarization. The reasons for aging can be divided into three groups, namely the loss of active materials, the loss of lithium and the deterioration of ionic kinetics [10].

The evolution of passive layers, i.e. the solid electrolyte interphase (SEI) at the anode and the solid permeable interphase at the cathode (SPI), takes on a key role in the aging of lithium-ion cells [11]. Whereas the SEI ideally prevents any further reduction of the electrolyte at the anode after formation, the electrolyte is continuously oxidized at the cathode due to the SPI's incapability of full passivation [12–14]. As the thickening and reconstruction of passive layers consume active lithium, there is a direct correlation to capacity loss [15–20]. Under extreme operational conditions such as a high state of charge (SoC) or high temperatures, these layers can even isolate active material by growing into its porous structure or clog the separator's pores [16,21].

* Corresponding author. Tel.: +49 89 289 26969; fax: +49 89 289 26968.
E-mail address: simon.schuster@tum.de (S.F. Schuster).

http://dx.doi.org/10.1016/j.est.2015.05.003
2352-152X/

At the cathode, a high delithiation degree, e.g. $x < 0.35$ for $Li_xNi_{1/3}Mn_{1/3}Co_{1/3}O_2$ (NMC) or $x < 0.5$ for Li_xCoO_2 (LCO), may result in irreversible structural changes, named rock salt structure, leading to an irreversible capacity loss [17,22,23]. Lithium cations move to the anode releasing electrons when charging a lithium-ion cell, which results in an increase of vacancies in the lithium layers. Thereby, repulsion forces between encompassing transition metal layers rise due to the missing virtue of compensation. Due to similar ionic radii, 0.76 Å for Li^+ and 0.67 Å for Ni^{2+}, the latter tend to migrate to the lithium layers and compensate the repulsion forces between transition metal layers by filling these vacancies irreversibly [24]. As a consequence, released oxygen promotes the oxidation of electrolyte leading to a further growth of the SPI. In addition, due to the higher conductivity of the SEI compared to the combination of SPI and rock salt structure, the cathode is assigned the main portion of charge transfer resistance [12,25]. With an increase of oxygen vacancies, the dissolution of the cathode is promoted. As a consequence, oxidation products migrate to the anode where they are reduced and catalyze the growth of the SEI by forming electron conducting tunnel paths [17]. For NMC cells, most of the oxidation products detected at the anode is manganese, but there are also traces of nickel and cobalt [26]. Whereas the anode material is principally not damaged by these deposits, ionic kinetics are deteriorated as a result [27–35]. In addition, cells cycled with high depths of discharge (DoD) seem to be more contaminated with oxidation products than cells stored at high SoC [36].

When lithium cations are inserted into or extracted from active material, the concomitant volumetric change, e.g. 10.2% for graphite anodes [37,38] and 3.4% for NMC transition metal layer cathodes [38,39], can lead to a loss of particles' bonds due to micro cracks or a loss of the contact of particles to the collector. It is assumed for graphite that especially the crossing of phase transitions results in erratic volumetric changes, indicating that also small DoD within an operational voltage window (ΔV) of phase transitions may lead to severe aging effects [33,34]. As the relative variation of graphite's lattice parameters in increased at two-phase reactions between different stages at the almost delithiated state, sliding and buckling of graphite planes must especially be considered when lithium-ion cells are discharged to very low SoC [37]. Such an irreversible structural disordering in the lattice of graphite leads to active material loss and thus, capacity loss of the anode. When the binding agent, typically polyvinylidendifluoride (PVDF), is decomposed, active materials may expand permanently facilitating a contact loss of particle to particle or collector [14,25]. As a consequence, active material gets isolated resulting in a loss of the electrode's capacity. In addition, passive layers may help to compensate volumetric changes but further capacity loss occurs if the layers break and need to be reconstructed [15,36,40].

At a high SoC, the potential of graphite anodes can come close to the critical value of 0 V vs. Li/Li^+. Low temperatures lead to a higher polarization due to slower diffusion processes and a hampered charge transfer. Thus, when charging lithium-ion cells at low temperatures with high currents, the graphite potential may drop below 0 V vs. Li/Li^+ [30,41]. As a consequence, lithium cannot be intercalated and is plated between active material and SEI. In [42], the thickness of a metallic lithium layer in plated lithium iron phosphate (LFP) based cells was measured to be 5 mm, which could even impose mechanical stress onto the cells' components. Facing a thermal runaway, plated lithium may lead to an increase of heat formation and so reduces the safety of a lithium-ion cell [43]. Theoretically, lithium plating is a reversible process as long as a conductive connection to graphite exists. As lithium oxidizes at about 100 mV vs. Li/Li^+, lower than the potential of deintercalation, plated lithium is removed in the subsequent discharge at first being apparent from a specific voltage plateau at the beginning [41,44,45]. This process is called stripping of plated lithium in which the ratio of LiC_6 and LiC_{12} stays constant until the deintercalation process starts [42,46]. In addition, it was spotted that during relaxation processes, plated lithium can oxidize to be chemically intercalated into graphite resulting in an increase of LiC_6 and reduction of LiC_{12} [46]. Although lithium plating is theoretically reversible, it is assumed that porous structures are formed during stripping and chemical intercalation processes, tending to lose the conductive connection to graphite [42,44–47]. In this case, isolated lithium may react with the electrolyte or damage the SEI resulting in a growth or reconstruction under accompanied capacity loss due to lithium consumption. In conclusion, when lithium plating occurs, one has to assume a mixture of stripping, chemical intercalation and isolation [42,44–47]. To avoid plating, a boost charging strategy, i.e. using high charging rates only at the beginning and reducing it at higher SoC is supposed to be a candidate for lowering the risk of this severe aging effect [48–50]. In addition, e.g. carbon black can improve the electrode's conductivity leading to a lower polarization but electrolyte additives used to stabilize the SEI growth as ethylene carbonate (EC) have shown to cause the opposite [16].

Most studies reveal a capacity fade for cells in storage with square root dependency on time [27,34,35,40,51]. The capacity under load is commonly reported to fade with a linear dependency on the charge throughput [34,35,40]. In rejection of these dependencies, enhanced aging upon prolonged cycling for distinct lithium-ion cells is observed in a few studies. Such a behavior for graphite based cells is e.g. described for cathodes comprising nickel, cobalt and aluminum (NCA) [52], LFP [33], NMC [34] and a blend of lithium manganese spinel (LMO) with NMC [36]. Possibly, these nonlinear aging characteristics are independent on the cathode chemistries but related to aging mechanisms of the anode. Instead of just observing enhanced aging upon prolonged cycling, only a handful of studies report about and explicitly address the origins of nonlinear aging characteristics [33,36,53,54].

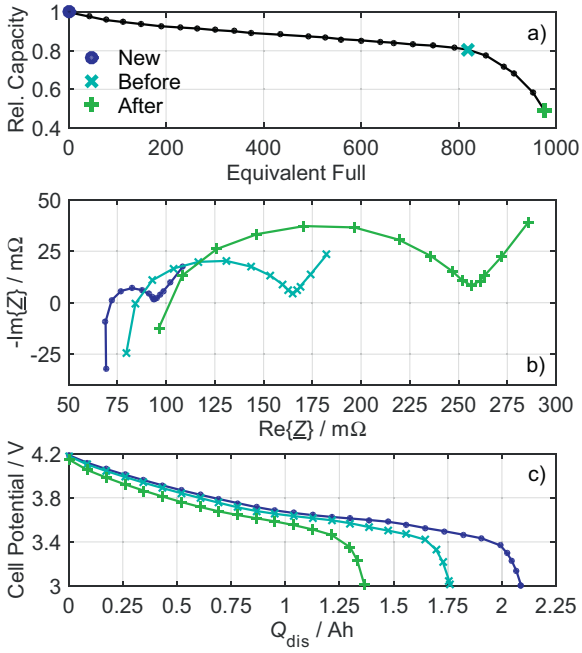

Fig. 1. (a) Development of the relative discharge capacity versus EFC for a graphite// NMC lithium-ion cell; (b) Nyquist plots of the impedance and (c) slow discharge curves referring to the three spots in (a): New cell (blue), before the start of nonlinear aging characteristics (cyan) and after the occurrence of these (green).

In Fig. 1(a), the development of the relative discharge capacity versus equivalent full cycles (EFC) is shown for a graphite//NMC lithium-ion cell elucidating the appearance of nonlinear aging characteristics upon prolonged cycling. The used load profile of the presented test case consisted of constant current (CC) charging with 0.5C until 4.2 V and CC discharging with 1C to 3.0 V at 35 °C and a break of 20 min between half cycles. Until a residual capacity of 80%, the assumption of a linear dependency on the charge throughput or EFC seems to be justified if first data points are neglected. In the literature, this turning point from linear to nonlinear aging characteristics is also observed at residual capacities of 80% or increased internal resistances of 150% [34,52]. By comparing the aging rate before and after the occurrence of nonlinear aging characteristics for the development of capacity in Fig. 1(a), an increase by factor seven can be estimated at minimum. In Fig. 1(b) and (c), Nyquist plots of the impedance and slow discharge curves with 0.02C are shown referring to the three spots in Fig. 1(a): New cell, before the start of nonlinear aging characteristics and after the occurrence of these. The degradation in terms of impedance increase and slow discharge capacity loss between 819 (before) and 977 EFC (after) far outweighs the one between 0 and 819 EFC and thus, principally correlates with the behavior of capacity.

It is assumed that the consumption of active lithium due to SEI growth is the driving force in the area of linear aging characteristics [32–35,52,53,55,56]. At the turning point, i.e. the start of nonlinear aging characteristics, lithium plating may occur even at moderate temperatures and charging rates due to a severe deterioration of ionic kinetics and graphite active material loss [17,33,34,37,52,53]. Furthermore, when plated lithium gets isolated by losing its conductive connection to graphite, this may further promote SEI growth which again deteriorates the anode's ionic kinetics. As this in turn promotes the occurrence of lithium plating, a circular process may arise with a severe loss of electrolyte due to a steady decomposition as a possible end [36,42,57]. This *self-reinforcing* ability of lithium plating has already been reported in [17,42].

In summary it can be said, therefore, that at a certain stage of cell's degradation, *aging induced lithium plating* may originate from:

1. reduced ionic kinetics of the graphite anode as a result of SEI growth
2. graphite active material loss

The occurrence of aging induced lithium plating leads to the turning point from linear to nonlinear aging characteristics. In [54], the appearance of nonlinear aging characteristics was observed after only 50 cycles at a temperature of −10 °C and could clearly be linked to lithium plating. As a result, it should be differentiated from a performance and an aging induced origin of lithium plating. On the other hand, plating itself must be separated into an irreversible (isolation) and a reversible (chemical intercalation, stripping) part.

Main aim of this work is to reveal effects of strongly nonlinear aging characteristics upon prolonged cycling for graphite//NMC based lithium-ion cells under different operational conditions. To avoid pronounced aging, the charging current, the DoD resp. ΔV and the temperature might be crucial, as the turning point from linear to nonlinear aging characteristics is assumed to be linked to lithium plating. To comprise all possible causes which could promote the occurrence of nonlinear aging characteristics, this work is based on a large aging experiment. In the sequel of this publication, nonlinear aging characteristics are investigated by a variety of electrochemical measurement techniques and post-mortem analyses.

2. Experimental

In this publication, mass-produced high-energy lithium-ion cells of the type Molicel IHR18650A by E-One Moli Energy Corp. with a nominal capacity of 1.95 Ah were investigated in terms of their cyclic aging behavior. The active materials of the cell comprise graphite on the negative and NMC on the positive electrode. A ΔV from 4.2 V to 3.0 V and maximum current rates of 1C or 2C for charging or discharging, respectively, are recommended by the manufacturer. In addition, the investigated type of cell has already been used in a pilot project BEV.

For the cycling of cells, the Cell Test System (CTS) by BaSyTec GmbH was used. Periodically, the experiment was stopped to measure the actual state of aging. Thereby, the CTS was used to measure the loss of capacity. The potentiostat VMP3 by Biologic Science Instruments was employed for electrochemical impedance spectroscopy (EIS). All measurements were conducted in climate chambers at 25 °C.

The actual capacity was always measured at first. Therefore, cells were charged with a CC of 0.5C, switching to a constant voltage (CV) phase at 4.2 V. When the current decreased below 0.1C in the CV phase, cells were defined as fully charged. After a break of 6 min, they were discharged with 1C until 3 V were reached. In a CV phase at 3 V, the lithium-ion cells were completely discharged until the current decreased below 0.05C. The CV phase in the discharging process served to eliminate the influence of impedance in the CC phase by a continuous depletion of polarization and thus, a better inference to active lithium in the cell is possible.

The impedance spectrum was measured in galvanostatic mode from 10 kHz to 10 mHz at an open circuit voltage of 3.68 V which corresponds to a SoC of approx. 50 %. Fig. 2 shows the Nyquist plot of a new cell and marks characteristic spots referring to concrete electrochemical processes which can be separated due to different time constants. In this work, the real part of the impedance at zero crossing, R_{zc}, and the resistance associated with passive layers and charge transfer, R_{pl+ct}, are used to quantify the amount of aging. The latter, which is the diameter of the envisaged half circle visible in the Nyquist plot, is defined as $R_{pl+ct} = \mathrm{Re}\{\underline{Z}_{total}\} - R_{zc}$. Usually, R_{zc} is mentioned as the ohmic resistance and is attributed to the sum of resistances of active materials, current collectors, electrolyte and separator [58–61]. For many other lithium-ion cells, two superimposed semi-circles are observed connecting R_{zc} and $\underline{Z}_{total}$ [62]. In the literature, the semi-circle at higher frequencies is commonly attributed to the passive layers [58–61]. The semi-circle at lower frequencies is attributed to the double layer capacity and the charge transfer resistance [58–61,63]. For this type of cell, only one semi-circle appears due to similar time constants of described processes. Therefore, R_{pl+ct} is further used to quantify aging effects of those processes in common. In addition, it is reported in the

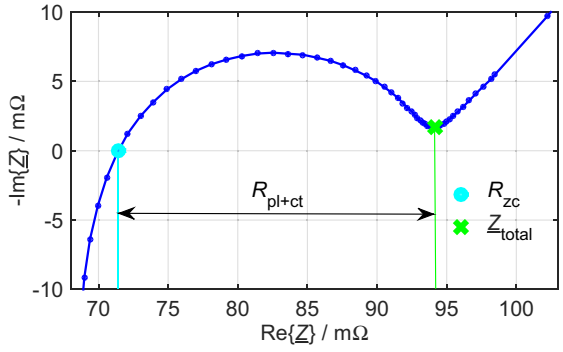

Fig. 2. Nyquist plot of a new cell at a SoC of 50% and 25 °C; R_{zc} and R_{pl+ct} are further used in this work to quantify the amount of aging.

Table 1
Aging matrix in dependency on the investigated parameters: ΔV, current rate and temperature.

Investigated parameter	ΔV / V	V_{max} / V	V_{min} / V	Charging rate (process) / C	Discharging rate / C	Temperature / °C
Voltage window ΔV	0.56 / 0.94 / 1.2	3.89 / 4.11 / 4.2	3.33 / 3.17 / 3.0	0.5 (CC)	1	35
	1.2 / 1.3	4.2 / 4.3	3.0 / 3.0	0.5 (CCCV)	1	35
Charging rate	1.2	4.2	3.0	0.2 / 0.5 / 1 (CCCV)	0.5	35
Discharging rate	1.2	4.2	3.0	0.5 (CCCV)	0.5 / 1 / 2	35
Temperature	1.2	4.2	3.0	0.5 (CCCV)	1	25 / 35 / 50
	0.94	4.11	3.17	0.5 (CC)	1	35 / 50

literature that the development of R_{pl+ct} is suitable to predict the appearance of nonlinear aging characteristics upon prolonged cycling [32].

For morphology characterization, new cells, cells before and after the turning point, which were cycled with a ΔV = 1.2 V at 35 °C with CC charging (0.5C) and CC discharging (1C), were investigated. The aging behavior of cells cycled with such a load profile was shown in Fig. 1. Cells were completely discharged to 3 V by CCCV until the current decreased below 0.1C and then opened in a glove box under controlled argon atmosphere. Samples of the electrodes were not rinsed and transported under vacuum to avoid contact with air. To investigate morphology modifications on μm-level, a Supra 25 scanning electron microscope (SEM) by Zeiss was used with an accelerating voltage of 15 kV. In addition, also SEM imaging itself was entirely carried out in vacuum.

Basically, cyclic aging depends on numerous parameters such as the ΔV, the mean SoC, the current rate of the charging and discharging process as well as the temperature. In this work, the mean SoC of all test cases is approximately 50% and thus, the effect of this parameter on the aging behavior is not further examined. Table 1 resumes the aging matrix in dependency on the investigated parameters, i.e. ΔV, the charging and discharging rate as well as the temperature. Cells were either charged only with a CC or with a CCCV process, whereas the termination condition for the latter is a current smaller 0.1C in the supplementary CV phase. All cells were discharged with CC. After a half cycle, always a break of 20 min was conducted. For all test cases which were executed from the start of the aging experiment, three cells were used to be able to average the aging behavior, exclude outliers, if necessary, and gain a statistically profound statement. For test cases which were started in the course of the experiment, only two cells were used as prior tests already revealed a homogeneous aging behavior of cells cycled with the same load profile at the same ambient conditions. Before the start of the aging experiment, cells were selected and preloaded with four mild cycles to avoid ongoing formation processes.

3. Results and discussion

As already mentioned, in the literature most aging studies of lithium-ion cells concentrate on the aging behavior above residual capacities of 80%. Fig. 3 shows the development of the relative discharge capacity versus EFC in dependency on ΔV for cells

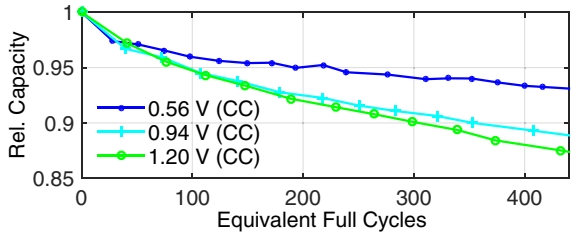

Fig. 3. Development of the relative discharge capacity versus EFC in dependency on ΔV; the abbreviations in the legend characterize the charging process.

charged (0.5C) and discharged (1C) with CC at 35 °C. The ΔV = 0.56 V, 0.94 V and 1.2 V correspond to a DoD = 27%, 73% and 87% for new cells, respectively, referring to the nominal capacity. Thereby, it has to be considered that the accumulated charge throughput per cycle decreases upon prolonged aging as polarization is increased due to growing impedances. Whereas the loss of capacity is increased with higher ΔV in Fig. 3, the assumption of a linear dependency on the charge throughput or EFC seems to be justified for all depicted test cases if first data points are neglected. Accordingly, a prediction of the aging behavior based upon data above residual capacities of 80% would overestimate the maximum reachable number of cycles as the occurrence of nonlinear aging characteristics upon prolonged cycling, as shown in Fig. 1(a), is neglected.

Therefore, in the following subchapters, the aging behavior upon prolonged cycling is presented for different operational conditions figuring out the effects on the turning point from linear to nonlinear aging characteristics. The following subchapters are divided into the effects of ΔV, current rate and temperature.

3.1. Nonlinear aging characteristics in dependency on ΔV

In this subchapter, the aging behavior upon prolonged cycling is presented for different ΔV. In addition to the test cases shown in Fig. 3, two load profiles with supplementary CV phase in the charging process, and thus longer periods at high SoC and deeper cycles, were added in order to provoke an early turning point from linear to nonlinear aging characteristics. These additional ΔV = 1.2 V and 1.3 V correspond to a DoD = 94% and 98% for new cells, respectively. Thereby, it is especially apparent from the test case ΔV = 1.3 V, that even for a broader ΔV than recommended, the accumulated charge throughput per cycle is smaller than the nominal capacity. Thus, the latter can only be gained by discharging with smaller currents, e.g. as shown in Fig. 1(c).

Fig. 4(a) shows the development of the relative discharge capacity versus EFC for different ΔV upon prolonged cycling. It is clearly visible that higher ΔV and supplementary CV phases in the charging process result in an earlier turning point. For test cases with CC charging, a reduction from ΔV = 1.2 V to 0.94 V extends the area of linear aging characteristics at about 42%. Otherwise, for test cases with CCCV charging, a reduction from ΔV = 1.3 V to 1.2 V results in a prolongation of about 46%. When comparing the test cases ΔV = 1.2 V with CC and CCCV charging, the longer periods at high SoC and deeper cycles result in a reduction of the number of EFC before the occurrence of the turning point of about 29%.

Fig. 4(b) and (c) show the development of R_{zc} and R_{pl+ct} versus EFC, respectively. Thereby, a strong reciprocal correlation to the development of the capacity is visible, i.e. a loss of capacity comes out with an appropriate rise of resistances and vice versa. As a consequence, there should be the possibility of perceiving or even predicting the occurrence of the turning point from impedance measurements. The correlation of resistances and capacity could e.g. be used on a battery management system (BMS) to detect nonlinear aging characteristics by the calculation of resistances regarding voltage drops caused by current pulses: As long as the gradient of the development of R is approximately constant, the

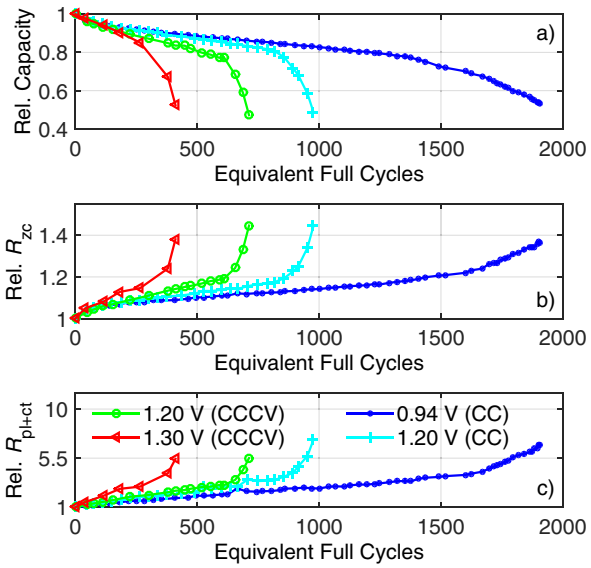

Fig. 4. (a) Development of the relative discharge capacity versus EFC in dependency on ΔV upon prolonged cycling; (b) and (c) show the development of R_{zc} and R_{pl+ct} versus EFC, respectively; the abbreviations in the legend characterize the charging process.

increase of R shows a linear dependency on the charge throughput but might turn to a nonlinear one when exceeding the measuring inaccuracy. In addition, it is apparent that the increase of R_{pl+ct} far outweighs the one of R_{zc}.

In order to clarify the reciprocal correlation of capacity and resistances, Fig. 5(a) shows R_{zc}, and Fig. 5(b), R_{pl+ct}, versus the corresponding values of capacity. It is apparent for both types of resistance, that even after the appearance of nonlinear aging characteristics, i.e. for residual capacities below approximately 80%, a linear relationship between resistances and capacity is discernible which represents a reciprocal correlation.

The reason for an earlier appearance of the turning point with an increase of ΔV could be a faster deterioration of ionic kinetics in the linear area. Higher SoC result in a thickening of the SEI and a stronger dissolution of the cathode, with oxidation products migrating to the anode and further promoting SEI growth under a steady consumption of active lithium as a result [32–35,52,55,56]. In addition, with higher ΔV, the graphite anode might increasingly suffer from loss of active material as erratic volumetric changes leading to irreversible structural disordering especially occur for lithium-ion cells discharged to very low SoC [37]. As the mean SoC is approximately 50% for all test cases, smaller ΔV also result in higher discharging cut-off voltages and thus, a smaller amount of graphite active material loss due to irreversible structural changes is expected. Therefore, aging induced lithium plating may occur earlier for test cases with higher ΔV and CV phases although the current rates while charging as well as the temperature are commensurate for load profiles depicted in Fig. 4.

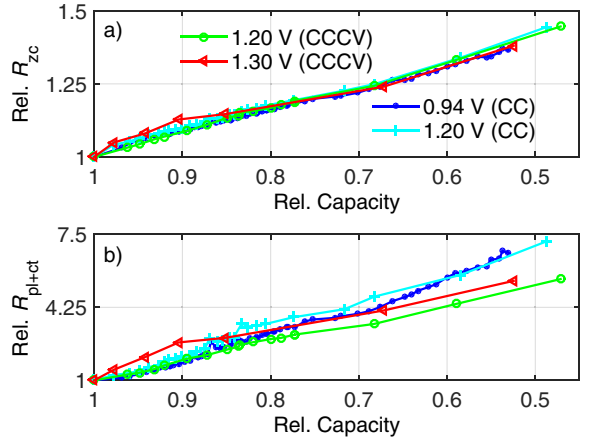

Fig. 5. Correlation of (a) relative R_{zc} and (b) relative R_{pl+ct} with the relative discharge capacity for all test cases in dependency on ΔV.

3.2. Nonlinear aging characteristics in dependency on the current rate

After the dependency on ΔV, the aging behavior upon prolonged cycling is shown for various charging and discharging rates. In compliance with Table 1, all test cases of this subchapter were conducted with ΔV = 1.2 V and CCCV charging at 35 °C. For test cases with different discharging or charging rates, the corresponding charging or discharging rate is 0.5C, respectively.

Fig. 6(a) shows the development of the relative discharge capacity versus EFC for different charging and discharging rates. For the test case with the maximum charging rate of 1C, the aging behavior shows nonlinear aging characteristics almost from the beginning of cycling. By reducing the charging rate to 0.5C, the maximum number of EFC until reaching the turning point can clearly be extended. For the minimum charging rate of 0.2C, no nonlinear aging characteristics are observed within the timeframe of this work.

For the test cases of different discharging rates, the correlation is contrary to charging against expectations: With higher rates of discharge, the turning point from linear to nonlinear aging characteristics seems to appear retarded. Although the extension of the linear area with 3% is marginal when comparing the discharging cases with 0.5C and 1C, there does not appear a turning point at all for the test case of 2C, even below residual capacities of 70%.

Fig. 6(b) and (c) show the development of R_{zc} and R_{pl+ct} versus EFC, respectively. Again as for the test cases in dependency on ΔV, a strong reciprocal correlation of capacity and resistances is visible. In addition, it is noteworthy that the shape of the development of

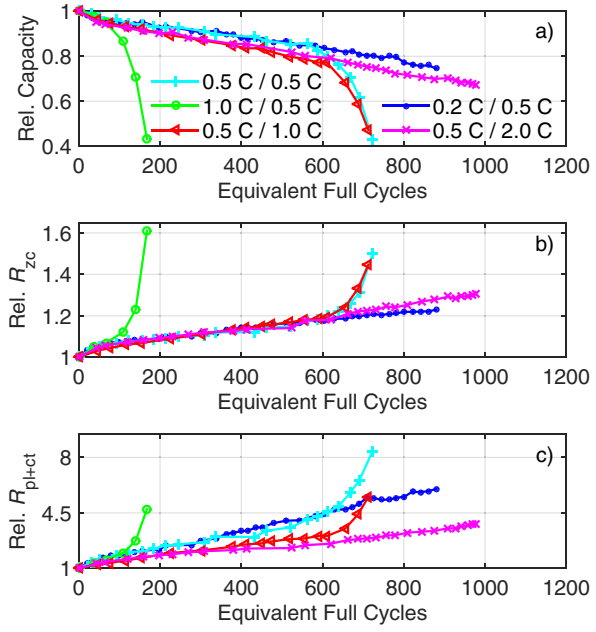

Fig. 6. (a) Development of the relative discharge capacity versus EFC in dependency on the current rate upon prolonged cycling; (b) and (c) show the corresponding development of R_{zc} and R_{pl+ct} versus EFC, respectively.

capacity and R_{zc} during the aging progress is almost the same for most of the test cases but then suddenly differs from a certain state of aging as a result of only a few cells show nonlinear aging characteristics at all. The slightly pronounced capacity loss before the turning point of cells which were discharged with higher rates could originate from the internal heat buildup whereby e.g. a maximum difference of 10 K is shortly detectable when comparing the cells of the discharging test case with 0.5C and 2C. Compared to Fig. 4, these observances are contrary as the aging behavior of all depicted test cases differed from the beginning but also all of them showed a turning point to nonlinear aging characteristics at residual capacities of approx. 80%. To spell out the relationship between resistances and capacity of Fig. 6, Fig. 7(a) and (b) show again R_{zc} and R_{pl+ct} versus the corresponding values of capacity.

The earlier appearance of the turning point with an increase of the charging rate can be explained by higher overpotentials resulting in an increased possibility that the potential of the anode drops below 0 V vs. Li/Li^+ [30]. Due to the formation of porous structures in plated lithium, the conductive connection between lithium and graphite can get lost resulting in an irreversible capacity decrease [44–47]. If plated lithium reacts with the electrolyte, this may further promote the growth of the SEI under lithium consumption resulting in deteriorated ionic kinetics which again facilitates lithium plating. In addition, it was shown for graphite//NMC lithium-ion cells by E-One Moli Energy Corp., that a mixture of electrolyte additives which synergistically prevent excessive SEI growth, extended the area of linear aging characteristics possibly by repressing the occurrence of lithium plating [32].

As the correlation for discharging is just contrary with higher rates leading to a retardation of the turning point, this behavior is maybe caused by an avoidance of strong delithiation degrees of the anode. Such a behavior occurred intensified for test cases with higher discharging rates due to higher overpotentials during the CC discharge. As a consequence of it, and due to the voltage controlled termination of the discharging process, resulting DoDs of test cases decrease with an increase of the discharging rates: For a rate of 0.5C, 1C and 2C, ensued DoDs are 98%, 94% and 76%, respectively. Additionally, these DoDs, which appear for the new state of cells, even are reduced during the progress of aging due to higher overpotentials which are caused by increased impedance parts.

Between half cycles, cells of all test cases always rested for 20 min. So, after a discharging process to the cut-off voltage of 3.0 V, the cell potentials can relax for 20 min before the start of the upcoming charging process. This relaxed value of cell potential can be used to estimate the delithiation degree of the anode after discharge. A high amount of residual lithium which cannot be

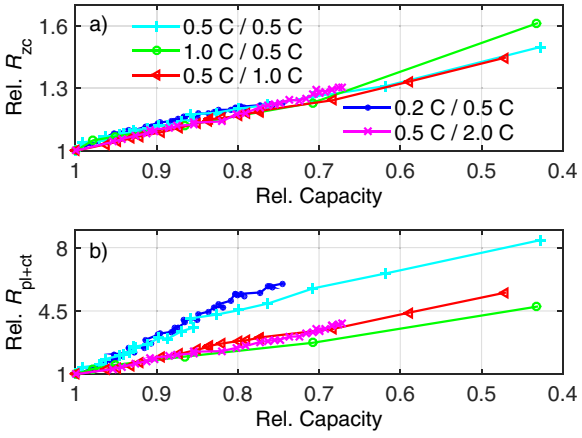

Fig. 7. Correlation of (a) relative R_{zc} and (b) relative R_{pl+ct} with the relative discharge capacity for all test cases in dependency on the current rate.

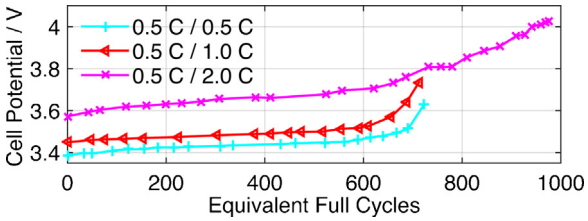

Fig. 8. Development of the relaxed cell potential in the discharged state of cells during the progress of aging for different discharging rates.

deintercalated from the anode leads to higher values of the relaxed cell potential after discharge. Fig. 8 shows the development of the relaxed cell potential in dependency from the discharging rate versus EFC. For the test cases of 0.5C and 1C discharging rate, the values of the cell potential after the 20 min break rose from 3.39 V and 3.45 V to 3.63 V and 3.74 V, respectively. In contrast, the cell potential after relaxation rose from 3.57 V to 4.03 V for the test case of 2C discharging rate – although no nonlinear aging characteristics appeared for this type of load. As a consequence of this, lower delithiation degrees of the anode may have resulted in less graphite active material loss [37]. In contrast, for an increase of the mean SoC also an enhanced growth of the SEI is imaginable, but graphite active material loss seemed to be dominating.

As a reduction of the anode's delithiation degree led to an avoidance of nonlinear aging characteristics, this effect was further examined by another experiment: Therefore, an additional test case with 0.5C / 1C with CCCV charging and CCCV discharging (2CCCV) was performed and compared to those only with CCCV charging or no CV phases at all. The additional test case with $\Delta V = 1.2$ V and synchronous CCCV charging and discharging resulted in a DoD = 103% for new cells referred to the nominal capacity. Termination condition in the CV phase at 3 V was a current smaller than 0.1C. In Fig. 9, it is clearly visible that the turning point of the test case with CCCV discharging appeared about 34% or 51% earlier referred to the test case with only CCCV charging or no CV phases at all. Thus, also this experiment emphasizes the detrimental effect of high delithiation degrees of the anode resp. cycling of lithium-ion cells to deep SoC.

In addition, the stripping of plated lithium could be another explanation for the turning point to be retarded with higher discharging rates. After plating has occurred, in the subsequent discharge, plated lithium oxidizes at first before the start of deintercalation as long as a conductive connection to graphite exists [44–46]. Although such a behavior of lithium-ion cells has not been reported in the literature yet, higher discharging rates could promote the stripping effect and thus, reducing the amount of irreversibly lost lithium due to plating.

3.3. Nonlinear aging characteristics in dependency on the temperature

As the effects of different ΔV and current rates give hints that lithium plating might be the cause for pronounced aging, the cyclic

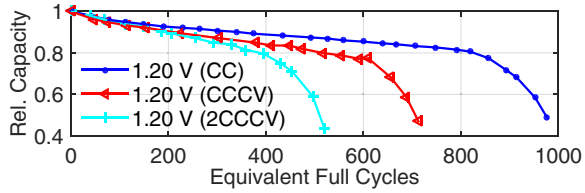

Fig. 9. Development of the relative discharge capacity versus EFC in dependency on the processes of cycling; the abbreviations in the legend characterize the charging process; 2CCCV represents a synchronous cycling with CCCV charging and discharging.

aging behavior in dependency on the temperature could further support this statement. In compliance with Table 1, a first set of test cases was conducted with $\Delta V = 1.2$ V with 0.5C CCCV charging and a discharging rate of 1C. Cells were cycled in self-built climate chambers at 25 °C, 35 °C and 50 °C. In addition, a second set of test cases with a milder $\Delta V = 0.94$ V and the same current rates was conducted at 35 °C and 50 °C.

Fig. 10(a) shows the development of the relative discharge capacity versus EFC for both sets of test cases. For the set with $\Delta V = 1.2$ V, cycling at the lowest temperature, i.e. 25 °C, results in the quickest occurrence of the turning point. In comparison, for the test case at 50 °C, the number of EFC before reaching the turning point is prolonged at about 8%. The test case between those boundaries, i.e. cycling at 35 °C, seems to be the optimum resulting in a prolongation of the linear area of roughly 40% referred to 25 °C. For the second set of test cases with $\Delta V = 0.94$ V, the capacity loss rate at 35 °C compared to 50 °C is smaller at first, but only for the test case at the lower temperature a turning point to pronounced aging appeared.

Fig. 10(b) and (c) shows the development of relative R_{zc} and R_{pl+ct} versus EFC. A reciprocal correlation compared to the development of the capacity is visible for all test cases and both resistances, except for the test case with $\Delta V = 0.94$ V at 50 °C. For this type of load, the increase of R_{zc} far outweighs the others and seems to stagnate at about 1100 EFC. It is assumed that time controlled aging mechanisms, i.e. calendric aging, led to a strong rise of R_{zc} but comparably low capacity loss for cycling with rather mild types of load but high temperatures. Such a behavior could originate from the growth of passive layers at high temperatures [16,21] and has already been reported for NMC cells cycled with very small currents over a longer period of time [64]. Fig. 11(a) and (b) show the correlation of R_{zc} and R_{pl+ct} with the corresponding values of the relative capacity, respectively. The assumption of a linear relationship between resistances and capacity is again justified except for the test case with $\Delta V = 0.94$ V at 50 °C. For this type of load, the stagnation of the increase of R_{zc} with ongoing capacity loss results in a nonlinear relation.

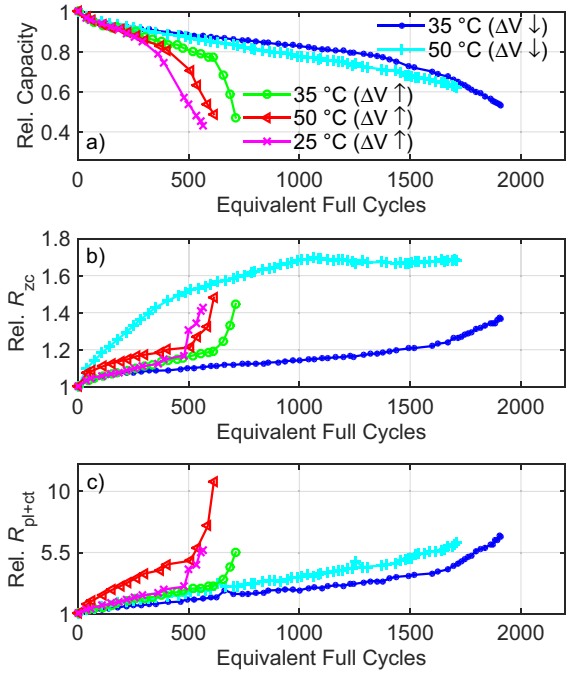

Fig. 10. (a) Development of the relative discharge capacity versus EFC in dependency on the temperature upon prolonged cycling; (b) and (c) show the corresponding development of R_{zc} and R_{pl+ct} versus EFC, respectively; the abbreviations in the legend characterize the test cases with $\Delta V = 1.2$ V (↑) and $\Delta V = 0.94$ V (↓).

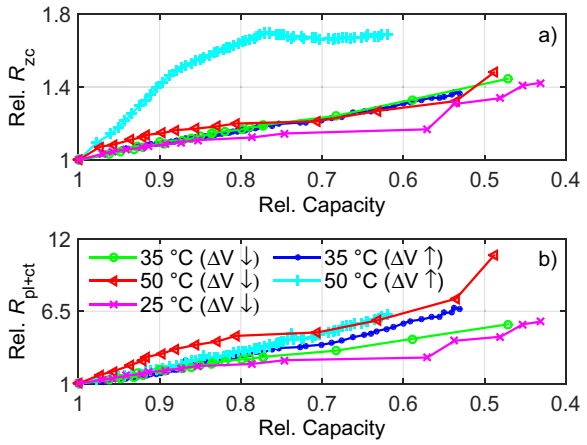

Fig. 11. Correlation of (a) relative R_{zc} and (b) relative R_{pl+ct} with the relative discharge capacity for all test cases in dependency on the temperature.

The earlier appearance of the turning point with lower temperatures is a strong signal for lithium plating to be the cause. Therefore, the aging behavior of different temperatures supports the assumptions gained by the test sets in dependency on ΔV and current rate. It was stated in the literature that below 25 °C, lithium plating has to be regarded as the dominant aging mechanism [30]. Above, the depletion of lithium inventory due to pronounced thickening of passive layers is the driving force [32]. Therefore, it was concluded in [30] that 25 °C is the optimum temperature for cycling lithium-ion cells leading to pronounced aging above and below. In principle, such a behavior can also be stated by the test cases cycled with $\Delta V = 1.2$ V shown in Fig. 10(a), but with a shift of the minimum to 35 °C indicating a strong susceptibility to lithium plating of the investigated type of cell.

3.4. Morphology characterization

The occurrence of the turning point is probably caused by deteriorated ionic kinetics and active material loss of the anode, both commonly leading to aging induced lithium plating. Therefore, the morphology of the graphite anode in contrast to the NMC cathode should exhibit modifications.

Fig. 12 presents SEM images of the NMC cathode at 5 k magnification for the three investigated states, i.e. Fig. 12(a) shows the morphology of a new cell, Fig. 12(b) of a cell before the start of nonlinear aging characteristics and Fig. 12(c) after the occurrence of these. In all images, the surface of the cathode seems to be unmodified and undamaged as no micro cracks or surface films are detectable.

When unrolling the aged graphite anodes, local areas of strong surface film formation were already visible by the human eye. The number and size of localized areas with modified morphology was found to be seriously increased for graphite anodes after the turning point compared to before. Such findings have already been reported in the literature for aged LFP based cells [33,42,53,54]. Fig. 13(a) shows the SEM image of the graphite anode of a new cell, in which the single particles in the order of 10 μm are clearly visible. In Fig. 13(b), the image of a well-preserved area for a cell before the turning point is shown, which is very similar to the one of a new cell. In contrast, also areas with strong surface film formations are detectable for the same state of aging depicted in Fig. 13(c). After the occurrence of the turning point, also the well-preserved areas seem to be covered with a thin surface film as shown in Fig. 13(d). Fig. 13(e) presents that the surface film in a

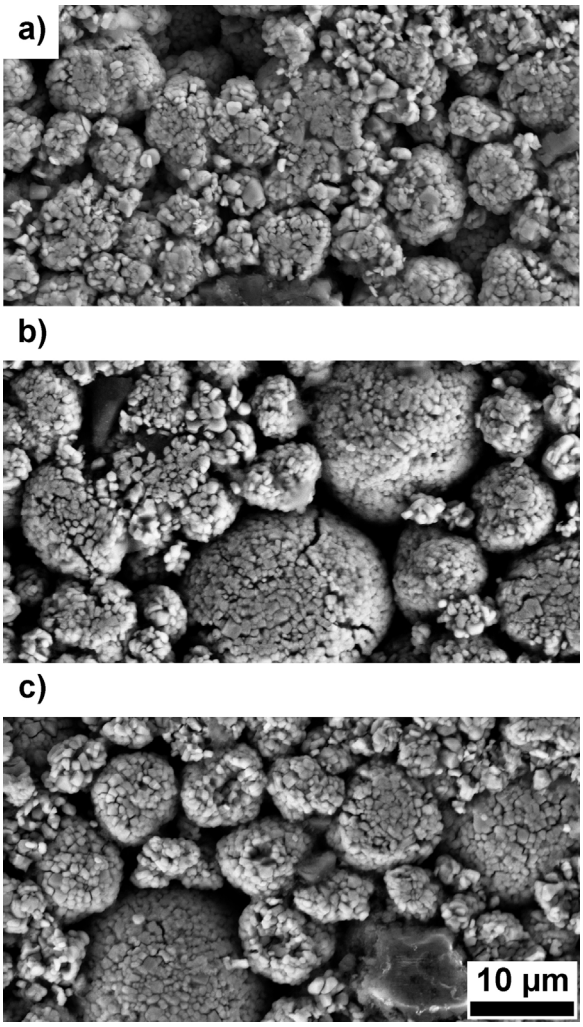

Fig. 12. SEM images of the NMC cathode at 5 k magnification for the three investigated states, i.e. (a) for a new cell; (b) before the start of nonlinear aging characteristics and (c) after the occurrence of these.

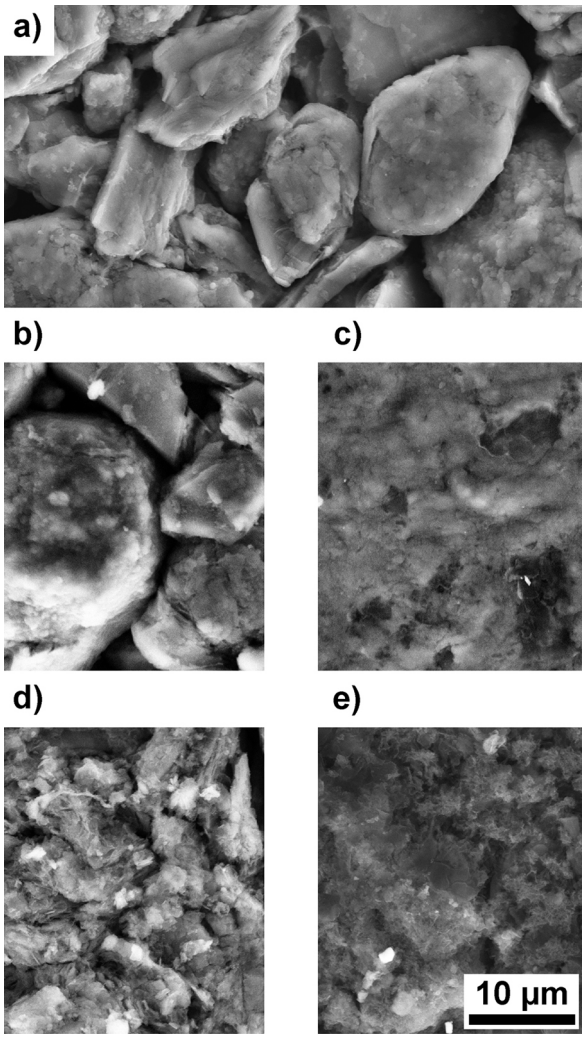

Fig. 13. SEM images of different positions of the unrolled graphite anode at 5 k magnification for the three investigated states; i.e. (a) for a new cell; (b) before the start of nonlinear aging characteristics in a well-preserved area; (c) before it in a strongly degraded area; (d) after it in a well-preserved area; (e) after it in a strongly degraded area.

strongly degraded area for a cell after the turning point even looks thicker compared to the one of a cell before. An explanation for these localized films could be SEI growth catalyzed by oxidation products from the cathode and by plated lithium reacting with the electrolyte. This can result in a circular process as the deterioration of ionic kinetics again promotes the occurrence of plating [32,46].

However, further tests have to be conducted to be able to prove aging induced lithium plating as the source of nonlinear aging characteristics. Based on the results which are presented in this publication, it can only be assumed as the turning point is provoked by high ΔV, high charging rates and low temperatures – which is also typical for the appearance of lithium plating in general. Therefore, to prove our proposed hypothesis, investigated cells will additionally be investigated by a variety of electrochemical measurement techniques and post-mortem analyses. Results of them will be presented in the sequel of this work.

4. Conclusion

In this publication, based on a widespread aging matrix, the aging behavior upon prolonged cycling was investigated for lithium-ion cells comprising graphite on the negative and NMC on the positive electrode. Whereas the capacity fade for cells under load is commonly reported to exhibit a linear dependency on the charge throughput, a turning point from linear to nonlinear aging characteristics is observed at residual capacities of about 80% under different operational conditions. It is assumed that in the linear area, passive layer growth leads to a deterioration of ionic kinetics under a steady consumption of active lithium. In addition, a loss of graphite active material is supposed to be caused by irreversible structural disordering especially when lithium-ion cells are discharged to very low SoC. For the turning point from linear to nonlinear aging characteristics, the occurrence of *aging induced lithium plating*, even at moderate charging rates and temperatures, might be the cause.

Results prove that the occurrence of nonlinear aging characteristics is facilitated by high charging rates, high ΔV and low temperatures. While the maximum charging rate of 1C led to enhanced aging almost from the beginning of cycling, no nonlinear aging characteristics were observed for the minimum charging rate of 0.2C. A reduction of ΔV from 1.2 V to 0.94 V extended the area of linear aging characteristics nearly about 42%. For the temperature, an increase from 25 °C to 35 °C resulted in an extension of almost 40% before reaching the turning point, but cycling at 50 °C compared to 35 °C reduced the maximum amount of EFC about 34%. Between the development of resistances and

capacity, a reciprocal correlation is observed even after the turning point, i.e. resistances show a pronounced increase after the occurrence of nonlinear aging characteristics. In addition, SEM images confirm that there is no modification of the morphology of the NMC cathode, but localized areas of the graphite anode are covered with thick surface films.

To get a deeper understanding of the mechanisms leading to the turning point from linear to nonlinear aging characteristics and to prove the described assumptions, cells are investigated by a variety of electrochemical measurement techniques and post-mortem analyses in the sequel of this publication. Techniques used in the sequel comprise e.g. incremental capacity analysis (ICA), X-ray diffraction (XRD), inductively coupled plasma optical emission spectroscopy (ICP-OES) and nuclear magnetic resonance (NMR) spectroscopy.

For reusing lithium-ion batteries exhausted upon electric vehicle operation in 2nd-life applications, the findings on nonlinear aging characteristics are of great importance. The key issue is to find the ideal hand-over time when a battery should be removed from the car and reused in the 2nd-life-application as stationary energy storage. Here, energy density is of minor importance and thus, storages can be oversized leading to very mild load profiles. As an outlook, it has to be investigated if the occurrence of nonlinear aging characteristics can be avoided or retarded by load reduction shortly before the kink. Due to an earlier appearance of the turning point with high charging rates and ΔV, but lower temperatures, the life of lithium-ion cells can possibly be extended by reducing the charging rate and ΔV, or increasing the temperature, just before the occurrence of nonlinear aging characteristics.

Acknowledgements

Funding from the German Federal Ministry for Economic Affairs and Energy (BMWi) of the EU-project ABattReLife and management by the German Aerospace Center (DLR) are gratefully acknowledged. The responsibility for this publication rests with the authors.

References

[1] Kraftfahrtbundesamt, Website of the German Federal Motor Transport Authority, http://www.kba.de/SharedDocs/Publikationen/DE/PM/2014/pm_02_14_fahrzeugzulassungen_12_2013_pdf.pdf?__blob=publicationFile&v=2 [Online, January 2014].
[2] H. Vikström, S. Davidsson, M. Höök, Lithium availability and future production outlooks, Appl, Energy 110 (2013) 252–266.
[3] A. Burke, Performance, Charging, and Second-use Considerations for Lithium Batteries for Plug-in Electric Vehicles. University of California, Institute of Transportation Studies, Research Report UCD-ITS-RR-09-17, Davis, 2009.
[4] E. Cready, J. Lippert, J. Pihl, I. Weinstock, P. Symons, R.G. Jungst, Technical and Economic Feasibility of Applying Used EV Batteries in Stationary Applications: A Study for the DOE Energy Storage Systems Program. U.S. Department of Energy, Sandia National Laboratories, Final Report SAND2002-4084, Albuquerque /Livermore (2003) .
[5] J. Neubauer, A. Pesaran, The ability of battery second use strategies to impact plug-in electric vehicle prices and serve utility energy storage applications, J. Power Sources 196 (2011) 10351–10358.
[6] C.K. Narula, R. Martinez, O. Onar, M.R. Starke, G. Andrews, Economic analyses of deploying used batteries in power systems, Final Report ORNL/TM-2011/151, U.S. Department of Energy, Oak Ridge National Laboratory, Oak Ridge, 2011.
[7] B. Williams, T. Lipman, Analysis of the combined vehicle- and post-vehicle-use value of lithium-ion plug-in-vehicle propulsion batteries. Task 3, Second life applications and value of traction lithium batteries, Final Report 500-02-004, University of California, Transportation of Sustainability Research Center, Berkeley, 2011.
[8] C.R. Standridge, L. Corneal, Remanufacturing, repurposing, and recycling of post-vehicle-application lithium-ion batteries. San José State University, Mineta National Transit Research Consortium, MNTC Report 12-20, San José, 2014.
[9] Y. Olofsson, M. Romare, Life Cycle Assessment of Lithium-ion Batteries for Plug-in Hybrid Buses. Chalmers University of Technology, Department of Energy and Environment/Department of Applied Physics, Report No. 2013:5, Göteborgg, Sweden.
[10] M. Kassem, J. Bernard, R. Revel, S. Pélissier, F. Duclaud, C. Delacourt, Calendar aging of a graphite/$LiFePO_4$ cell, J. Power Sources 208 (2012) 296–305.
[11] P. Balbueana, Y. Wang, Lithium-Ion Batteries – Solid-Electrolyte Interphase, first ed., World Scientific Pub Co., London, 2004.
[12] M. Shikano, H. Kobayashi, S. Koike, H. Sakaebe, Y. Saito, H. Hori, H. Kageyama, K. Tatsumi, X-ray absorption near-edge structure study on positive electrodes of degraded lithium-ion battery, J. Power Sources 196 (2011) 6881–6883.
[13] M.K. Rahman, Y. Saito, Investigation of positive electrodes after cycle testing of high-power Li-ion battery cells III: An approach to the power fade mechanism using FT-IR-ATR, J. Power Sources 174 (2007) 889–894.
[14] N. Dupré, J. Martin, J. Oliveri, P. Soudan, A. Yamada, R. Kanno, D. Guyomard, Relationship between surface chemistry and electrochemical behavior of $LiNi_{1/2}Mn_{1/2}O_2$ positive electrode in a lithium-ion battery, J. Power Sources 196 (2011) 4791–4800.
[15] S. Kim, A.C.T. van Duin, V.B. Shenoy, Effect of electrolytes on the structure and evolution of the solid electrolyte interphase (SEI) in Li-ion batteries: A molecular dynamics study, J. Power Sources 196 (2011) 8590–8597.
[16] V. Agubra, J. Fergus, Lithium Ion Battery Anode Aging Mechanisms, Mater. 6 (2013) 1310–1325.
[17] M. Broussely, P. Biensan, F. Bonhomme, P. Blanchard, S. Herreyre, K. Nechev, R.J. Staniewicz, Main aging mechanisms in Li ion batteries, J. Power Sources 146 (2005) 90–96.
[18] H.J. Ploehn, P. Ramadass, R.E. White, Solvent Diffusion Model for Aging of Lithium-Ion Battery Cells, J. Electrochem. Soc. 151 (2004) A456–A462.
[19] P. Röder, B. Stiaszny, J. Ziegler, N. Baba, P. Lagaly, H. Wiemhöfer, The impact of calendar aging on the thermal stability of a $LiMn_2O_4$-$Li(Ni_{1/3}Mn_{1/3}Co_{1/3})O_2$/graphite lithium-ion cell, J. Power Sources 268 (2014) 315–325.
[20] E. Sarasketa-Zabala, I. Gandiaga, L.M. Rodriguez-Martinez, I. Villarreal, Calendar ageing analysis of a $LiFePO_4$/graphite cell with dynamic model validations: Towards realistic lifetime predictions, J. Power Sources 272 (2014) 45–47.
[21] J. Vetter, P. Novák, M.R. Wagner, C. Veit, K.-C. Möller, J.O. Besenhard, M. Winter, M. Wohlfahrt-Mehrens, C. Vogler, A. Hammouche, Ageing mechanisms in lithium-ion batteries, J. Power Sources 147 (2005) 269–281.
[22] M. Wohlfahrt-Mehrens, C. Vogler, J. Garche, Aging mechanisms of lithium cathode materials, J. Power Sources 127 (2004) 58–64.
[23] J. Choi, A. Manthiram, Role of Chemical and Structural Stabilities on the Electrochemical Properties of Layered $LiNi_{1/3}Mn_{1/3}Co_{1/3}O_2$ Cathodes, J. Electrochem. Soc. 152 (2005) A1714–A1718.
[24] D. Mohanty, H. Gabrisch, Microstructural investigation of LixNi1/3Mn1/3Co1/3O2 ($x \leq 1$) and its aged products via magnetic and diffraction study, J. Power Sources 220 (2012) 405–412.
[25] J. Zhou, P.H.L. Notten, Studies on the degradation of Li-ion batteries by the use of microreference electrodes, J. Power Sources 177 (2008) 553–560.
[26] F. Lin, I.M. Markus, D. Nordlund, T. Weng, M.D. Asta, H.L. Xin, M.M. Doeff, Surface reconstruction and chemical evolution of stoichiometric layered cathode materials for lithium-ion batteries, Nat. Commun. 5 (2014) Art. 3529.
[27] S. Grolleau, A. Delaille, H. Gualous, P. Gyan, R. Revel, J. Bernard, E. Redondo-Iglesias, J. Peter, Calendar aging of commercial graphite/$LiFePO_4$ cell - Predicting capacity fade under time dependent storage conditions, J. Power Sources 255 (2014) 450–458.
[28] B. Stiaszny, J.C. Ziegler, E.E. Krauß, M. Zhang, J.P. Schmidt, E. Ivers-Tiffée, Electrochemical characterization and post-mortem analysis of aged $LiMn_2O_4$-NMC/graphite lithium ion batteries part II: Calendar aging, J. Power Sources 258 (2014) 61–75.
[29] J. Wang, Y. Tang, J. Yang, R. Li, G. Liang, X. Sun, Nature of $LiFePO_4$ aging process: Roles of impurity phases, J. Power Sources 238 (2013) 454–463.
[30] T. Waldmann, M. Wilka, M. Kasper, M. Fleischhammer, M. Wohlfahrt-Mehrens, Temperature dependent ageing mechanisms in Lithium-ion batteries - A Post-Mortem study, J. Power Sources 262 (2014) 129–135.
[31] L. Bodenes, R. Naturel, H. Martinez, R. Dedryvère, M. Menetrier, L. Croguennec, J. Pérès, C. Tessier, F. Fischer, Lithium secondary batteries working at very high temperature: Capacity fade and understanding of aging mechanisms, J. Power Sources 236 (2013) 265–275.
[32] J.C. Burns, A. Kassam, N.N. Sinha, L.E. Downie, L. Solnickova, B.M. Way, J.R. Dahn, Predicting and Extending the Lifetime of Li-ion Batteries, J. Electrochem. Soc. 160 (2013) A1451–A1456.
[33] M. Klett, R. Eriksson, J. Groot, P. Svens, K.C. Högström, R.W. Lindström, H. Berg, T. Gustafson, G. Lindbergh, K. Edström, Non-uniform aging of cycled commercial $LiFePO_4$//graphite cylindrical cells revealed by post-mortem analysis, J. Power Sources 257 (2014) 126–137.
[34] M. Ecker, N. Nieto, S. Käbitz, J. Schmalstieg, H. Blanke, A. Warnecke, D.U. Sauer, Calendar and cycle life study of Li(NiMnCo)O2-based 18650 lithium-ion batteries, J. Power Sources 248 (2014) 839–851.
[35] J. Wang, J. Purewal, P. Liu, J. Hicks-Garner, S. Soukazian, E. Sherman, A. Sorenson, L. Vu, H. Tataria, M.W. Verbrugge, Degradation of lithium ion batteries employing graphite negatives and nickel-cobalt-manganese oxide + spinel manganese oxide positives: Part 1 aging mechanisms and life estimation, J. Power Sources 269 (2014) 937–948.
[36] D.A. Stevens, R.Y. Ying, R. Fathi, J.N. Reimers, J.E. Harlow, J.R. Dahn, Using High Precision Coulometry Measurements to Compare the Degradation Mechanisms of NMC/LMO and NMC-Only Automotive Scale Pouch Cells, J. Electrochem. Soc. 161 (2014) A1364–A1370.
[37] T. Ohzuku, Y. Iwakoshi, K. Sawai, Formation of Lithium-Graphite Intercalation Compounds in Nonaqueous Electrolytes and Their Application as a Negative

Electrode for a Lithium Ion (Shuttlecock) Cell, J. Electrochem. Soc. 140 (1993) 2490–2498.
[38] W.H. Woodford, W.C. Carter, Y. Chiang, Design criteria for electrochemical shock resistant battery electrodes, Energy Environ. Sci. 5 (2012) 8014–8024.
[39] W. Yoon, K.Y. Chung, J. McBreen, X. Yang, A comparative study on structural changes of $LiCo_{1/3}Ni_{1/3}Mn_{1/3}O_2$ and $LiNi_{0.8}Co_{0.15}Al_{0.05}O_2$ during first charge using in situ XRD, Electrochem. Commun. 8 (2006) 1257–1262.
[40] J. Schmalstieg, S. Käbitz, M. Ecker, D.U. Sauer, A holistic aging model for Li (NiMnCo)O2 based 18650 lithium-ion batteries, J. Power Sources 257 (2014) 325–334.
[41] B. Bitzer, A. Gruhle, A new method for detecting lithium plating by measuring the cell thickness, J. Power Sources 262 (2014) 297–302.
[42] M. Petzl, M. Kasper, M. Danzer, Lithium plating in a commercial lithium-ion battery - A low-temperature aging study, J. Power Sources 275 (2015) 799–807.
[43] M. Fleischhammer, T. Waldmann, G. Bisle, B. Hogg, M. Wohlfahrt-Mehrens, Interaction of cyclic ageing at high-rate and low temperatures and safety in lithium-ion batteries, J. Power Sources 274 (2015) 432–439.
[44] R.V. Bugga, M.S. Smart, Lithium Plating Behavior in Lithium-Ion Cells, ECS Trans. 36 (2010) 241–252.
[45] N. Legrand, B. Knosp, P. Desprez, F. Lapicque, S. Rael, Physical characterization of the charging process of a Li-ion battery and prediction of Li plating by electrochemical modelling, J. Power Sources 245 (2014) 208–216.
[46] V. Zinth, C. von Lüders, M. Hofmann, J. Hattendorff, I. Buchberger, S. Erhard, J. Rebelo-Kornmeier, A. Jossen, R. Gilles, Lithium plating in lithium-ion batteries at sub-ambient temperatures investigated by in situ neutron diffraction, J. Power Sources 271 (2014) 152–159.
[47] M. Petzl, M.A. Danzer, Nondestructive detection characterization, and quantification of lithium plating in commercial lithium-ion batteries, J. Power Sources 254 (2014) 80–87.
[48] B. Lunz, Z. Yan, J.B. Gerschler, D.U. Sauer, Influence of plug-in hybrid electric vehicle charging strategies on charging and battery degradation costs, Energy Policy 46 (2012) 511–519.
[49] S.S. Zhang, The effect of the charging protocol on the cycle life of a Li-ion battery, J. Power Sources 161 (2006) 1385–1391.
[50] P.H.L. Notten, J.H.G. Op het Veld, J.R.G. van Beek, Boostcharging Li-ion batteries: A challenging new charging concept, J. Power Sources 145 (2005) 89–94.
[51] M.B. Pinson, M.Z. Bazant, Theory of SEI Formation in Rechargeable Batteries: Capacity Fade, Accelerated Aging and Lifetime Prediction, J. Electrochem. Soc. 160 (2013) A243–A250.
[52] K. Smith, J., Neubauer, E., Wood, M., Jun A. Pesaran, National Renewable Laboratory Website, http://www.nrel.gov/docs/fy13osti/58550 pdf [Online, April 2013].
[53] E. Sarasketa-Zabala, F. Aguesse, I. Villarreal, L.M. Rodriguez-Martinez, C.M. López, P. Kubiak, Understanding Lithium Inventory Loss and Sudden Performance Fade in Cylindrical Cells during Cycling with Deep-Discharge Steps, J. Phys. Chem. C 119 (2015) 896–906.
[54] M. Ouyang, Z. Chu, L. Lu, J. Li, X. Han, X. Feng, G. Liu, Low temperature aging mechanism identification and lithium deposition in a large format lithium iron phosphate battery for different charge profiles, J. Power Sources 286 (2015) 309–320.
[55] T. Baumhöfer, M. Brühl, S. Rothgang, D.U. Sauer, Production caused variation in capacity aging trend and correlation to initial cell performance, J. Power Sources 247 (2014) 332–338.
[56] M. Dubarry, C. Truchot, M. Cugnet, B.Y. Liaw, K. Gering, S. Sazhin, D. Jamison, C. Michelbacher, Evaluation of commercial lithium-ion cells based on composite positive electrode for plug-in hybrid electric vehicle applications. Part I: Initial characterization, J. Power Sources 196 (2011) 10328–10335.
[57] E. Sarasketa-Zabala, I. Gandiaga, E. Martinez-Laserna, L.M. Rodriguez-Martinez, I. Villarreal, Cycle ageing analysis of a $LiFePO_4$/graphite cell with dynamic model validations: Towards realistic lifetime predictions, J. Power Sources 275 (2015) 573–587.
[58] C.T. Love, M.B.V. Virji, R.E. Rocheleau, K.E. Swider-Lyons, State-of-health monitoring of 18650 4S packs with a single-point impedance diagnostic, J. Power Sources 266 (2014) 512–519.
[59] K. Takeno, M. Ichimura, K. Takano, J. Yamaki, S. Okada, Quick testing of batteries in lithium-ion battery packs with impedance-measuring technology, J. Power Sources 128 (2004) 67–75.
[60] D. Andre, M. Meiler, K. Steiner, C.h. Wimmer, T. Soczka-Guth, D.U. Sauer, Characterization of high-power lithium-ion batteries by electrochemical impedance spectroscopy. I. Experimental investigation, J. Power Sources 196 (2011) 5334–5341.
[61] W. Waag, S. Käbitz, D.U. Sauer, Experimental investigation of the lithium-ion battery impedance characteristic at various conditions and aging states and its influence on the application, Appl. Energy 102 (2013) 885–897.
[62] D. Andre, M. Meiler, K. Steiner, H. Walz, T. Soczka-Guth, D.U. Sauer, Characterization of high-power lithium-ion batteries by electrochemical impedance spectroscopy. II: Modelling, J. Power Sources 196 (2011) 5349–5356.
[63] A. Jossen, Fundamentals of battery dynamics, J. Power Sources 154 (2006) 530–538.
[64] H.M. Smith, J.C. Dahn, Long-Term Low-Rate Cycling of $LiCoO_2$/Graphite Li-Ion Cells at 55 °C, J. Electrochem Soc. 159 (2012) A705–A710.